# Density Functional Theory Study of Tetrathiafulvalene and Thianthrene in Acetonitrile: Structure, Dynamics, and Redox Properties†

**Joost VandeVondele,*,‡ Ruth Lynden-Bell,‡ Evert Jan Meijer,§ and Michiel Sprik‡**

*Department of Chemistry, University of Cambridge, Lensfield Road, Cambridge CB2 1EW, United Kingdom, and van't Hoff Institute for Molecular Sciences, Universiteit van Amsterdam, Nieuwe Achtergracht 166, NL-1018 WV Amsterdam, The Netherlands*

*Received: August 26, 2005; In Final Form: October 4, 2005*

The redox potentials of the organic compounds tetrathiafulvalene (TTF) and thianthrene (TH) in an explicit aprotic polar solvent, acetonitrile, have been computed using ab initio molecular dynamics simulation based on a Gaussian basis set methodology. The density functional description of the pure solvent yields a diffuse and mobile liquid, with structural and dynamical properties that are in good agreement with earlier classical models and experiment. Molecular dynamics simulation of both solute species in their neutral and radical cation states combined with free energy difference calculations result in estimates for the redox potentials of the reactions $TH^{\bullet+} + TTF \rightarrow TH + TTF^{\bullet+}$ and $TH^{2+} + TTF^{\bullet+} \rightarrow TH^{\bullet+} + TTF^{2+}$. The obtained values are $0.95 \pm 0.06$ and $1.09 \pm 0.06$ V, respectively, in excellent agreement with experimental data of 0.93 and 1.08 V. Our computational approach is based on Marcus theory, assuming quadratic free energy surfaces. We show that this approximation can still be accurate in systems, such as TH, that undergo a significant change in geometry upon oxidation. Furthermore, despite the different localization of the spin density in the radical cations, results based on self-interaction-corrected functionals and on standard generalized gradient approximations are identical to within 10 meV.

## 1. Introduction

Reduction or oxidation of molecules is an elementary step in many chemical processes. The redox potentials of many compounds are known experimentally and provide a direct measure of the free energy cost of adding or removing electrons from a species and thus of their relative stability. Redox energies are the condensed-phase equivalents of the electron affinities and ionization potentials in the gas phase, with the presence of the solvent playing a crucial role. The role of the solvent and its influence on the rate of electron transfer was made particularly clear by Marcus in his treatment of electron-transfer reactions.[1,2] Linking the microscopic world of atomistic simulation to the macroscopic experimental and theoretical results, i.e., computing reaction energies and rates, remains a significant challenge. The required microscopic statistical mechanics and classical molecular simulation techniques have been established previously,[3−6] but a parameter-free approach based on ab initio molecular dynamics simulations with explicit solvent molecules has only been explored recently.[7−10] This can be attributed in part to the significant computational cost of ab initio molecular dynamics simulations. However, this computational cost is compensated for by the fact that the underlying density functional theory (DFT) description is able to model accurately quantities such as solvent response and polarization, solute conformational changes, and the vertical energy gaps of the compounds. Furthermore, the combination of DFT with molecular dynamics (MD) directly takes into account the solvent fluctuations and reorganizations that are crucial for reactions in solution, as we showed in our previous work which focused on transition metal aqua ions ($Ag^+/Ag^{2+}$ in refs 7 and 8, $Cu^+/Cu^{2+}$ in ref 8, $Ru^{2+}/Ru^{3+}$ in ref 9, and $MnO_4^-/MnO_4^{2-}$ and $RuO_4^-/RuO_4^{2-}$ in ref 10). The same questions will be addressed in the present study, but now for two typical redox-active organic molecules, tetrathiafulvalene (TTF) and thianthrene (TH) (Figure 1) in a representative aprotic solvent, namely, acetonitrile (MeCN). A second more technical issue concerns the nature of the electronic states and the accuracy of the density functional approach. The redox-active states in coordination complexes remain localized on the central metal ion and its ligands in both the reduced and the oxidized state as we verified in refs 7−10. However, the relevant electronic states in molecular solutions such as the model systems studied here are of a rather different nature. The neutral (reduced) species is a stable closed shell molecule, while the oxidized species is a radical cation. The electron hole can be delocalized over several atomic centers in the molecule (in our case sulfur and carbon atoms) but, unlike for the transition metal ions, is (usually) not shared with solvent molecules. However, electron holes in the standard density functional models used in ab initio simulation (the generalized gradient approximation) have a tendency to spread out too much, which can lead to partial transfer to the solvent and even to formation of hemi-bonds with the solvent such as has been observed for the OH radical.[11,12] The source of this erroneous behavior is the self-interaction error (SIE)[13,14] to which radicals are particularly sensitive.[15,16] Here, we investigate this error and employ a recently proposed self-interaction correction (SIC) scheme[12] together with standard density functionals so that a direct comparison can be made. This empirical SIC scheme was applied to hemi-bonded radical cation dimers of He, $NH_3$, $H_2O$, HF, and Ne and to the $^{\bullet}OH$−water interaction. The performance for radical cations of larger molecules is therefore a necessary

† Part of the special issue "Michael L. Klein Festschrift".

* Author to whom correspondence should be addressed. Phone: 44-1223763874. E-mail: jv244@cam.ac.uk.

‡ University of Cambridge.

§ Universiteit van Amsterdam.

10.1021/jp054841+ CCC: $33.50 
Published on Web 11/09/2005

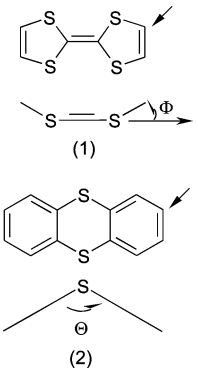


**Figure 1.** Top and side view of tetrathiafulvalene (1) and thianthrene (2). The arrows in the top views indicate the reference carbon atom for the analysis of solvent structure in section 5. The out-of-plane deformation angle $\Phi$ and the folding angle $\Theta$ are defined in the side views of 1 and 2, respectively.

and instructive test. We will show that quantitative agreement with experimental redox potentials can be obtained for the full reactions $TH^{\bullet+} + TTF \rightarrow TH + TTF^{\bullet+}$ and $TH^{2+} + TTF^{\bullet+} \rightarrow TH^{\bullet+} + TTF^{2+}$ and that the self-interaction error in these reaction free energies cancels.

The model systems that we have chosen, TTF and TH (depicted in Figure 1), are interesting targets for such a calculation. TTF in particular is a versatile compound and a strong electron donor. As described in detail in ref 17 and references therein, its properties have been exploited in the first "organic metal", in organic superconductors, in various charge-transfer complexes, in macromolecular structures for molecular shuttles and switches, and in nonlinear optics and sensors. The ability to predict the redox properties of this and derived compounds is thus of significant practical value. So far, theoretical calculations on TTF have focused on gas-phase structures and energetics[18−21] and the band structure in a molecular crystal.[22] TH has fewer experimental applications but has been considered as a charge transport material in electronic devices[23] or as a model compound in photoinduced electron transfer.[24] Additionally, its butterfly shape (Figure 1) has triggered a number of theoretical investigations.[25−27]

MeCN is a commonly employed aprotic solvent that has not yet been characterized by ab initio molecular dynamics simulation. In the context of electron-transfer reactions, it is noteworthy that MeCN is a typical solvent in dye-sensitized solar cells.[28,29] A number of classical models are available for MeCN. The model of Böhm and co-workers[30] is a rigid six-site model and is often employed as a reference model. However, three-site models are commonly used as well.[31,32] More recent parametrizations introduce intramolecular degrees of freedom and polarizability.[33−37] Electronic structure calculations on acetonitrile have focused on the geometries and interaction energies of the dimer and on small clusters.[36,38−40] Also of interest are recent simulations using a mixed quantum classical description of naphthalene, coumarin 153, and chlorophyll-a in acetonitrile, which address the solvent structure[41,42] and redox potentials,[43] respectively.

In this paper, we briefly review the statistical mechanics behind the computation of redox potentials in section 2 and provide the details of our computations in section 3. The structure, dynamics, and polarization of pure acetonitrile are discussed in section 4. Molecular structure, conformational changes, and electronic structure of the solutes in solution and their interaction with the solvent are described in section 5. The computed redox potentials are compared with experiment in section 6, and results are summarized in section 7.

## 2. Calculation of Redox Potentials

Redox potentials are directly proportional to the free energy difference between the oxidized and the reduced state.[5,10] The oxidation free energy ($\Delta A$) is rigorously given by the thermodynamic perturbation relation[44]

$$\Delta A = -k_B T \ln\left\langle \exp\left(-\frac{\Delta E(\{R_I\})}{k_B T}\right)\right\rangle_R \quad (1)$$

$$= k_B T \ln\left\langle \exp\left(\frac{\Delta E(\{R_I\})}{k_B T}\right)\right\rangle_O \quad (2)$$

where the vertical ionization energy ($\Delta E$) is defined as

$$\Delta E(\{R_I\}) = E_O(\{R_I\}) - E_R(\{R_I\}). \quad (3)$$

$E_R(\{R_I\})$ and $E_O(\{R_I\})$ are the total energy of the system for a given set of ionic coordinates $\{R_I\}$ in the reduced (R) and respectively oxidized (O) state with one electron less. As usual, $k_B$ is the Boltzmann constant, and $T$ the temperature. $\langle\cdots\rangle_R$ and $\langle\cdots\rangle_O$ denote canonical averages over the reduced and oxidized potential energy surface. Equations 1 and 2 are exact but are impractical for direct evaluation. Through the use of umbrella sampling techniques they can nevertheless be evaluated.[5]

Electron-transfer (redox) reactions for which Marcus theory holds are a special but important class of systems for which a more manageable expression can be derived.[3−5] Introducing the probability distributions $P_R(\Delta E)$ and $P_O(\Delta E)$ of observing ionic configurations with a given $\Delta E$ in the reduced and oxidized state, respectively, we can rewrite eqs 1 and 2 as

$$\Delta A = -k_B T \ln \int \exp\left(-\frac{\Delta E}{k_B T}\right) P_R(\Delta E)\, d\Delta E \quad (4)$$

$$= k_B T \ln \int \exp\left(\frac{\Delta E}{k_B T}\right) P_O(\Delta E)\, d\Delta E \quad (5)$$

This expression can now be approximated by assuming that in the cumulant expansion of $P_X(\Delta E)$, X = R or O, only the first few cumulants are nonzero.[44,45] Truncating the cumulant expansion at some finite order might introduce a systematic error in the estimation of $\Delta A$ but can, for a given finite amount of data, reduce significantly the statistical error in the estimate. The harmonic (quadratic) approximation underlying Marcus theory assumes that only the first two cumulants are nonzero and thus that the distribution $P_X(\Delta E)$ is Gaussian. In this case, the oxidation free energy is given by

$$\Delta A = \Delta A_R = \Delta E_R - \frac{1}{2k_B T}\sigma_R^2 \quad (6)$$

$$= \Delta A_O = \Delta E_O + \frac{1}{2k_B T}\sigma_O^2 \quad (7)$$

where $\Delta E_R$ and $\Delta E_O$ are the average and $\sigma_R^2$ and $\sigma_O^2$ are the variance of the distributions $P_X$, X = R or O. So, $\Delta E_X$, X = R or O, is given by

$$\Delta E_X = \int \Delta E P_X(\Delta E)\, d\Delta E = \langle \Delta E(\{R_I\})\rangle_X \quad (8)$$

and similarly $\sigma_X^2$ by

$$\sigma_X^2 = \int (\Delta E - \Delta E_R)^2 P_X(\Delta E)\, d\Delta E = \langle (\Delta E(\{R_I\}) - \Delta E_X)^2\rangle_X \quad (9)$$

The three expressions $\Delta A_R$, $\Delta A_O$ are only identical if the harmonic approximation is exactly satisfied. In that case, it can be shown (see, for example, ref 10) that $\sigma_R^2 = \sigma_O^2$, and hence summing eqs 6 and 7 and dividing by 2 we can also write

$$\Delta A = \Delta A_C = \frac{1}{2}(\Delta E_R + \Delta E_O) \tag{10}$$

The advantage of $\Delta A_C$ is that only the averages and not the fluctuations of $\Delta E$ need to be sampled, providing a statistically robust estimate. The downside of this expression is that it requires MD simulations on both oxidized and reduced potentials. However, if two simulations have been performed, then the quality of the harmonic approximation can be verified by comparing the three available expressions. In this work, we emphasize the value of the expressions $\Delta A_R$ or $\Delta A_O$ that allow for redox estimates based on a single canonical simulation. Within the harmonic approximation, it is also straightforward to compute the reorganization free energy ($\lambda$) that is given by

$$\lambda = \lambda_R = \frac{\sigma_R^2}{2k_B T} \tag{11}$$

$$= \lambda_O = \frac{\sigma_O^2}{2k_B T} \tag{12}$$

$$= \lambda_C = \frac{1}{2}(\Delta E_R - \Delta E_O) \tag{13}$$

### 3. Computational Setup

The molecular dynamics simulations involved the following systems: liquid acetonitrile (the pure solvent), solvated TH and TTF, and the solvated radicals $TH^{\bullet+}$ and $TTF^{\bullet+}$. Initially, 45 molecules of acetonitrile were equilibrated classically at constant volume and 298 K using a rigid six-site model of acetonitrile.[30] The cubic unit cell has edges of 15.74 Å, which is equivalent to a density of 786.6 g/L. The same periodic unit cell has been used for the model solutions containing a single solute molecule with TH($TH^{\bullet+}$) and TTF($TTF^{\bullet+}$) replacing 3 and 2 acetonitrile molecules, respectively.

All density functional calculations have been performed with the freely available CP2K/Quickstep program.[46,47] The program is based on a hybrid Gaussian and plane wave scheme in which the wave functions are expanded using a Gaussian basis set, and an auxiliary basis of plane waves is employed to expand the density.[48] This method allows for an efficient and accurate evaluation of the total energy, Kohn−Sham matrix, and ionic forces.[47] The Becke exchange and the Lee−Yang−Parr correlation functional[49,50] (BLYP) have been used in almost all calculations, except where the functional by Perdew, Burke, and Ernzerhof[51] (PBE) is mentioned explicitly. Pseudopotentials of the Goedecker−Teter−Hutter (GTH) type, based on the parametrization of Hartwigsen−Goedecker−Hutter[52,53] and adapted for the density functional, have been used for all atoms. A split valence Gaussian basis set designed specifically for these pseudopotentials,[47] of triple-$\zeta$ quality and with two sets of polarization functions (TZV2P), has been employed for all atoms including hydrogen. It has been shown previously for simulations of liquid water that this basis set yields converged structural and dynamical properties.[54] Here, by comparison of results of simulations with a smaller basis set, double-$\zeta$ quality with one set of polarization functions (DZVP), we demonstrate convincingly that this also holds true for our simulations of liquid acetonitrile. In all calculations, matrix elements are considered negligible if the overlap matrix element of the corresponding basis functions are smaller than $10^{-12}$. The size of the auxiliary basis was determined by using a 200 Ry plane wave density cutoff.

The self-interaction-corrected (SIC) density functional calculations used the scaled spin density SIC first employed in ref 12. Referring to d'Avezac et al.[55] the scaled SIC (SS) is used within a restricted open shell scheme; i.e., for paired spins the $\beta$ wave functions have the same spatial extent as the $\alpha$ wave functions. The SS approach introduces an additional term in the Kohn−Sham energy functional

$$E_{sic}^{SS} = -aE_H[m] - bE_{XC}[m,0] \tag{14}$$

Here, $m = \rho_\alpha - \rho_\beta$ is the spin density, $E_H[m]$ and $E_{XC}[m, 0]$ are the Hartree and exchange−correlation energy of this density, and $a$ and $b$ are empirical parameters. The introduction of these scaling factors is an important distinction with the approach of ref 55. We use the previously determined[12] values of $a = 0.2$ and $b = 0.0$ in this work, unless a different value is mentioned explicitly. $-E_H[m]$ is exactly the exchange energy of the unpaired electron with itself (self-interaction energy). The exchange with the other electrons is approximated by the GGA. Note that the value of $a = 0.2$ is similar to the scaling factor of the Hartree−Fock exchange used in Becke's B3LYP functional.[56,57]

Ab initio molecular dynamics (MD) simulations used the Born−Oppenheimer method with a time step of 0.5 fs in the microcanonical (NVE) ensemble. The molecular dynamics simulations of the radical systems were carried out using the scaled SIC energy functional. During MD simulations, an initial guess for the wave functions is generated using a density matrix extrapolation scheme (PS extrapolation) with order $k = 2$.[47] Wave functions are optimized with the orbital transformation (OT) method,[58] which provides an efficient and robust way to deal with radicals, systems that can be more difficult to converge otherwise. For the oxidized systems a conjugate gradient minimization scheme was employed, whereas a direct inversion in the iterative subspace (DIIS) scheme was used for the uncharged systems. The convergence criterium for the gradient is $3 \times 10^{-7}$. On average, 7 iterations are needed to reach convergence for the neutral systems, whereas 26 steps are needed for the radical systems. The energy conservation during MD is excellent, with a drift of the total energy of the radical systems of $10^{-6}$ au/(ps atom), which is equivalent to a temperature drift of about 2 K in 10 ps. Systems have been simulated for 12, 11, 11, 8, and 8 ps for pure MeCN, solvated TTF, TH, $TTF^{\bullet+}$, and $TH^{\bullet+}$, respectively. The simulations of pure MeCN using the smaller basis set (DZVP) had durations of 8 and 15 ps using BLYP and PBE, respectively. The neutral systems have been started from the corresponding classical configurations, whereas the radical system runs are a continuation from an equilibrated frame of the ab initio simulation of the neutral system. Properties have been computed after discarding the first 2 ps for equilibration.

Finally a note about system size effects and periodic boundary conditions. Our model systems consist of a single redox-active solute. No explicit (physical) counterions are included. The charge of the oxidized species is balanced by the neutralizing background provided by the Ewald summation technique used to compute the long-range forces. This homogeneous background can be considered as an artificial but nonetheless real counterion as we have argued in our previous work on transition metal ions. Clearly, the interaction of a charge with its periodic images and the neutralizing background leads, for the small

system sizes typical of ab initio MD, to a significant dependence of total energies on system dimensions. Furthermore, there is the fundamental issue that the zero of the potential within periodic boundary conditions is arbitary[59] and can only be defined by comparing to a (semi)-finite system with a realistic interface (e.g., solvent/vacuum or solvent/electrode, for a first attempt in aqueous solution see ref 60). The redox free energy of half-reactions as computed using this approach have therefore no physical meaning and cannot be compared to experimental redox potentials. The same holds for the reaction free energies of full reactions except for reactions that preserve the charge states of the ions, i.e., when reactant and product ions have the same charge. In that case long-range interactions can be expected to cancel. The validity of this cancellation of errors is supported by the good agreement with experimental reaction free energies that we obtained for the $Ag^{2+} + Cu^{+} \rightarrow Ag^{+} + Cu^{2+}$ reaction in ref 8 and $MnO_4^- + RuO_4^{2-} \rightarrow MnO_4^{2-} + RuO_4^-$ in ref 10. The full reactions between TTF and TH molecules are of the same type, and we have good reason to expect that the same cancellation applies. Consistent with the various estimators introduced in section 2 for the half-reaction free energies, we can define therefore corresponding estimators for the redox free energies for the $TH^{\bullet+} + TTF \rightarrow TH + TTF^{\bullet+}$ reaction

$$\Delta\Delta A_X^1 = \Delta A_X^{TTF} - \Delta A_X^{TH} \tag{15}$$

where X = R or O and the $\Delta A_X$ are the oxidation free energies of eqs 6 and 7. The superscript 1 has been added to distinguish the reaction free energy of eq 15 from the free energy for the $TH^{2+} + TTF^{\bullet+} \rightarrow TH^{\bullet+} + TTF^{2+}$ reaction

$$\Delta\Delta A_X^2 = \Delta A_X^{TTF^{\bullet+}} - \Delta A_X^{TH^{\bullet+}} \tag{16}$$

where the $\Delta A_X$ are again the oxidation free energies of the radical cations.

## 4. Liquid Acetonitrile

The liquid structure as characterized by the pair correlation functions is shown in Figure 2. In the following discussion and in the figures, we denote the methyl carbon and central carbon by CC and CN, respectively. Discrepancies between BLYP DFT calculations using DZVP and TZV2P basis sets are very small. This level of agreement demonstrates that structural properties of the liquid at ambient temperature and fixed volume are well converged with these basis sets. Previous simulations of liquid water, computationally a more demanding liquid, lead to similar conclusions.[54] Furthermore, PBE and BLYP calculations yield very similar results. Agreement with the pair-potential-based results is good, in particular for the pronounced CC−N peak, shown in the upper panel of Figure 2. However, the discrepancies for the CN−CN and the N−H pair correlation functions are an indication of small differences in the local liquid structure. In particular, for the N−H pair correlation function, shown in the lowest panel of Figure 2, the ab initio simulations exhibit a broader first peak with an earlier onset. This difference can be related to the tendency of the classical molecules to interact with two H atoms belonging to the same methyl group in a bidentate configuration with the N atom of another molecule. The majority of the configurations observed in the DFT simulations have a single H−N interaction per N−CC contact. The difference in the CN−CN pair correlation (center panel) is more intriguing, as a shoulder that is present in the classical simulations is absent in the DFT description. The first shoulder in the classical model can be attributed to antiparallel dimers,

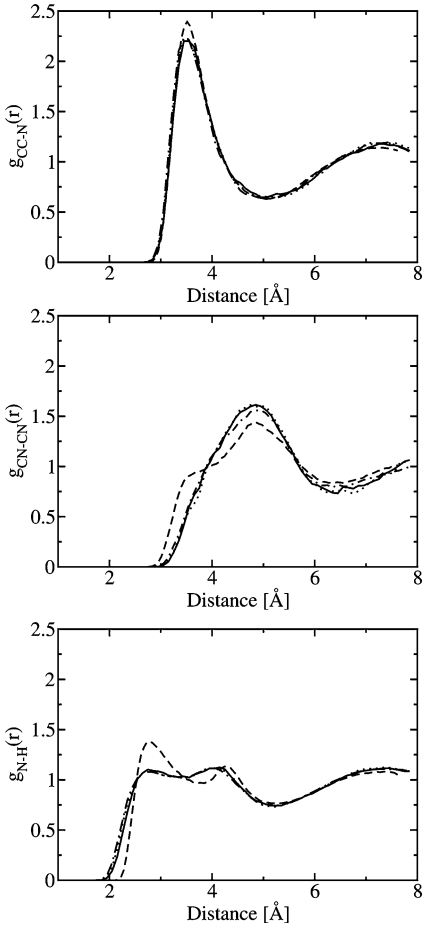


**Figure 2.** Selected pair correlation functions in liquid acetonitrile as obtained from simulations of 45 molecules at approximately 300 K: methyl carbon−nitrogen (upper panel), central carbon−central carbon (middle panel), and nitrogen−hydrogen (lower panel). A dashed line indicates results based on pair potentials, whereas the solid and dotted lines are for BLYP simulations using TZV2P and DZVP basis sets. respectively, and dash−dotted lines are for PBE simulations with a DZVP basis set. The different density functionals and basis sets yield results that are nearly indistinguishable.

whereas the main peak is mostly dimers in a head−tail configuration. The relative energies of these configurations in the gas-phase dimers, as obtained with the classical model and the PBE and BLYP functionals, seem insufficient to explain the differences in the solvent structure. Indeed, the classical value for the relative energy (8 kJ/mol) is between the BLYP (6 kJ/mol) and the PBE (10 kJ/mol) results. We note that the PBE result is in good agreement with accurate MP2 calculations (11 kJ/mol).[38,39]

The diffusion constant $D$ and the reorientational correlation time $\tau_2$ have been computed to probe the dynamical properties of the liquid as described using BLYP. The self-diffusion coefficient ($D$) is estimated from the slope of the mean-square displacement (MSD) of the molecules versus time

$$6D = \lim_{t\to\infty} \frac{d}{dt} \langle |\Delta R_i(t)| \rangle \tag{17}$$

The mean-square displacement in shown in Figure 3. The diffusion constant is obtained as the slope of the linear fit to the data in the range 1.5−6 ps and is $2.15 \times 10^{-5}$ cm$^2$/s. The experimental value[61] at 313 K and 0.1 MPa is $5.01 \times 10^{-5}$ cm$^2$/s, in fair agreement with the simulation results. Experimentally, a diffusion constant approximately equal to our simulation

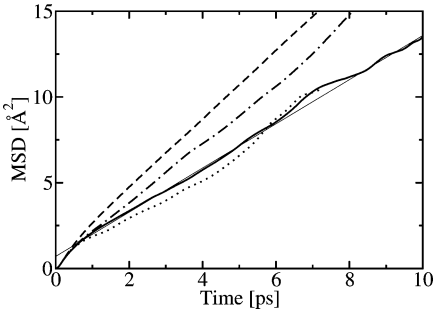


**Figure 3.** Mean-square displacement (MSD) in liquid acetonitrile. A dashed line indicates results based on pair potentials, whereas the solid and dotted lines are for BLYP simulations using TZV2P and DZVP basis sets, respectively, and a dash−dotted line is for PBE simulations with a DZVP basis set. The thin solid line is a linear fit to the BLYP TZV2P data in the 1.5−6 ps interval.

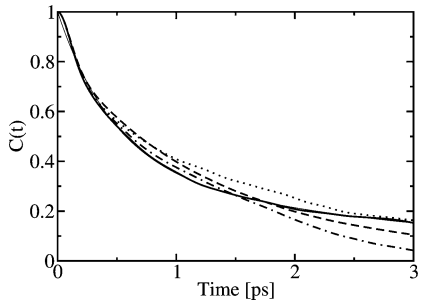


**Figure 4.** Orientational time correlation function in liquid acetonitrile. A dashed line is employed for the result based on pair potentials, whereas the solid and dotted lines are for BLYP simulations using TZV2P and DZVP basis sets, respectively, and a dash−dotted line is for PBE simulations with a DZVP basis set. The thin solid line, nearly indistinguishable, is a three-parameter fit to the BLYP TZV2P data (see text).

results is observed at 253 K and 0.1 MPa or 313 K and 251.2 MPa. The diffusion constant obtained with the classical model for the same system size and density (Figure 3), based on a trajectory of 100 ps at 298 K, is $3.32 \times 10^{-5}$ cm$^2$/s. This is smaller than the literature value of $4.3 \times 10^{-5}$ cm$^2$/s obtained for the same model at 291 K for a system size of 125 molecules and 20 ps simulation time and could be indicative of system size effects.[30,62]

The integral over the orientational correlation function [$C_2(t)$] has been used as an estimate of the orientational correlation time $\tau_2$

$$\tau_2 = \int_0^\infty \mathrm{d}t \, \langle P_2[e_i(t)e_i(0)] \rangle \qquad (18)$$

where $P_2(x) = {}^1/_2(3x^2 - 1)$ and $e_i$ is the unit vector in the CC−N direction. To compute the integral, we have performed a fit of the data in the interval 0−3 ps using

$$C_2(t) \approx a_1 \exp(-t/t_1) + (1 - a_1)\exp(-t/t_2) \qquad (19)$$

which yields coefficients $a_1 = 0.62$, $t_1 = 0.47$ ps, and $t_2 = 3.30$ ps. The correlation function and this fit are shown in Figure 4. The resulting correlation time $\tau_2 = 1.53$ ps. This is again in fair agreement with experimental values of around 1.25 ps for $CD_3CN$.[63,64] The value that we obtain from the classical model using the same procedure is 1.2 ps, slightly larger than the published results (1.0 ps).

The relatively high diffusion and the short orientational correlation time of the DFT liquid are very convenient from a computational perspective. Indeed, the properties sampled over a trajectory will converge more rapidly than the same property in a liquid with lower diffusion and longer orientational correlation times, such as, for example, water.

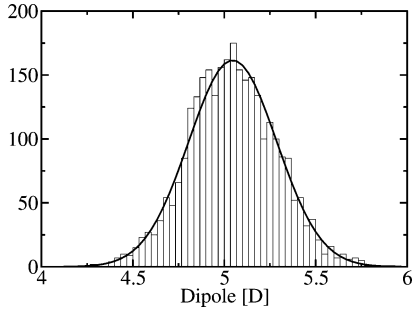


**Figure 5.** Histogram of the molecular acetonitrile dipoles in the liquid as computed using maximally localized Wannier functions. The full line is a Gaussian fit.

Finally, we analyze the distribution of the molecular acetonitrile dipole moments in the liquid computed from the centers of the maximally localized Wannier functions.[65,66] We note that, with this method, the calculated dipole of an isolated acetonitrile molecule in the gas phase is 4.08 D, in good agreement with standard calculations (4.04 D, using BLYP and a 6-31+G** basis), experiment (3.92 D),[67] and the classical model employed in this work (4.14 D).[30] The results for the liquid have been obtained from an analysis of 80 frames (3600 molecular dipoles), separated by 125 fs, and are shown in Figure 5. We find that the distribution of the molecular dipole moments is approximately Gaussian with an average value of 5.05 D and a standard deviation of 0.24 D. The average value of the dipole in the liquid is thus increased by 25% relative to the gas-phase dipole. This should be compared to the 60% enhancement observed in liquid water.[66] The value obtained here is slightly higher than 4.7 D obtained for a cluster of eight molecules[40] and the 4.5 D derived from modeling experimental absorption spectra of liquid acetonitrile[68] but quite similar to the value of 4.9 D obtained with a classical polarizable potential.[33]

## 5. Structure of Tetrathiafulvalene and Thianthrene in Solution

Gas-phase calculations on TH predict a ground-state geometry of butterfly shape with a folding angle around the S−S axis (see Figure 1 for a definition) of ∼129°, in good agreement with a recent X-ray structure.[25−27,69] However, in benzene solution and in an ordering liquid (Merck Nematic Phase IV) folding angles of ∼140° have been reported.[70,71] Our results in the liquid, shown in the upper panel of Figure 6, are consistent with this shift to larger angles. The average value of the folding angle ∼136°, which is, given the limited sampling of this relatively low frequent mode, in agreement with these measurements in liquids. Our finite temperature results also indicate that a broad range of angles (110−160°) is sampled, but flat configurations are not observed on our 10 ps time scale, consistent with the calculated barrier of 20.9 kJ/mol.[27] Neutral TTF adopts a boat shape geometry in the gas phase, with a deformation angle of the five-membered ring (see Figure 1 for a definition) of 15.6−18.5° depending on the theoretical method employed and a small energy cost for planarization of ∼2 kJ/mol.[18] As shown in the lower panel of Figure 6 both boat and flat configurations are sampled at ambient temperatures, with similar probabilities.

TH and TTF undergo a conformational change upon oxidation, resulting in a geometry that is, on average, flat. This is

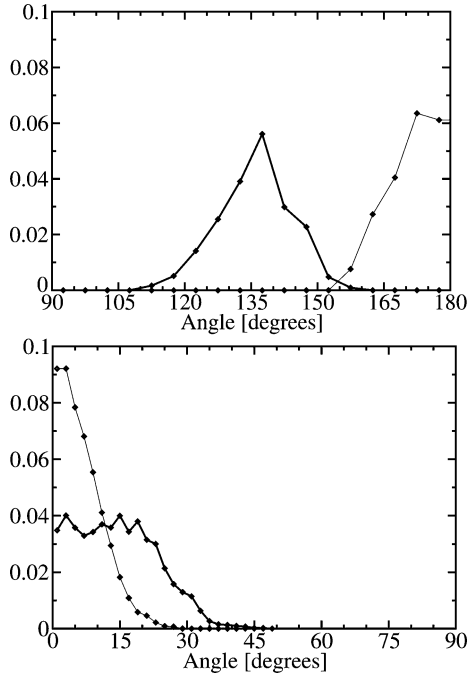


**Figure 6.** Characterization of the butterfly shape of thianthrene (upper panel, folding angle as defined in Figure 1) and the boat shape of tetrathiafulvalene (lower panel, deformation angle of Figure 1) in their neutral states (thick lines) and the flattening of both molecules in their radical cation states (thin lines).

observed in our simulations (Figure 6) and known from previous calculations in the gas phase.[18,20,21,25−27] The conformational change is most significant for TH, since the two configurations have only very limited overlap. (Note that the $\pi$ system of the TH dication is isoelectronic with anthracene and therefore formally an aromatic system, which could explain the preference for a planar structure.) The trajectory of the radical cation has been initiated from an equilibrated neutral configuration and thus provides, within an adiabatic approximation, an estimate of the time needed for the conversion from a butterfly configuration to a flat configuration upon oxidation. We find that this is a fast process going from the initial 138° to 180° in just 160 fs. Furthermore, the oscillation is strongly damped, since the amplitudes in the following two oscillations are approximately 170° and 165°, well within the thermally accessible range. Finally, earlier calculations on $TTF^{2+}$ have shown that this species adopts a configuration where the two rings are rotated by ∼37.8° with respect to each other.[72,21] The barrier for rotation around the connecting bond is less than 4 kJ/mol. We have not performed explicit MD simulations of $TTF^{2+}$, but this suggests that the two rings rotate relatively freely at ambient temperature.

The solvent structure around the solutes along with the change in solvent structure upon oxidation is characterized using selected pair correlation functions in Figure 7. The solvation is relatively unstructured. Pair correlation functions do not display a peak higher than 1.5 units. A similar structure has been observed with semiempirical molecular mechanics calculations of naphthalene and coumarin 153 in acetonitrile.[41,42] For both solutes in the neutral state, we observe a preferential orientation of the acetonitrile methyl group toward the sulfur atom, with the nitrogen pointing away from it. The preference for such an orientation is reduced near the carbon atoms of the rings. The average acetonitrile orientation is reversed upon oxidation, giving rise to a clear peak in the N−S pair correlation functions. This change is most pronounced for TH. In contrast the rearrangement near the carbon atoms of the rings is relatively

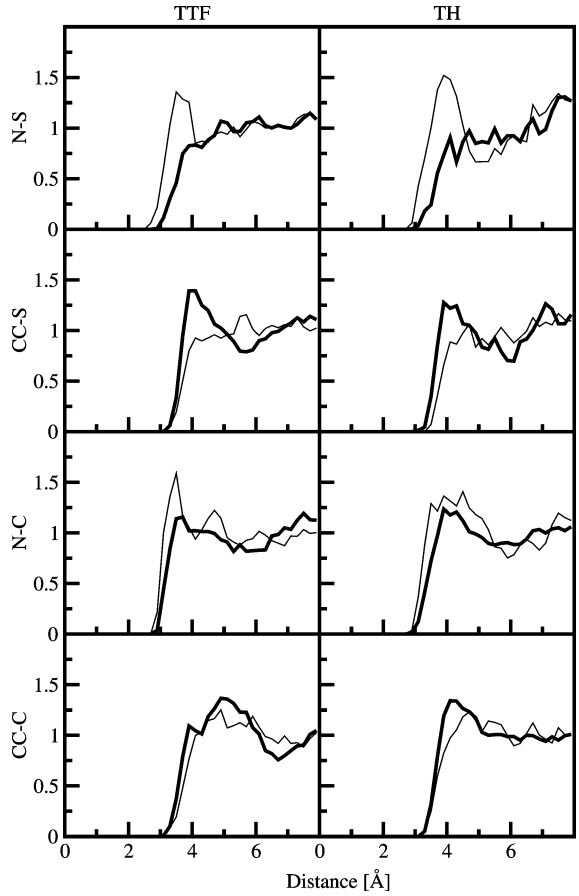


**Figure 7.** Solvent−solute pair correlation functions for tetrathiafulvalene (left) and thianthrene (right) in acetonitrile. Thick solid lines refer to the neutral state, while thin solid lines refer to the radical cation state of the solutes. The distribution around the sulfur (S) atom of the solute, which carries the largest spin density in the cation state, is shown in the top two panels, whereas the lower two panels show the distribution around selected solute carbon (C) atoms, indicated by arrows in Figure 1. Pair correlation functions are computed with respect to the acetonitrile nitrogen (N) and methyl carbon (CC).

small, for TH as well as TTF. As we will show below, this is consistent with the fact that the largest amount of spin density is located near the sulfur atoms.

The spin density, i.e., the difference between the α and $\beta$ electron density, of the radical cations is visualized in Figure 8. It is positive everywhere, since the electronic structure is computed with the scaled SIC approach, which is a restricted open shell method. The spin density is delocalized over several atoms of the solute but not of the solvent. The most pronounced accumulation of the spin density is on the S atoms of the TH solute. This is quantified using a Mulliken spin population analysis in Figure 9. The average spin population of a sulfur atom is 0.15 and 0.28 for $TTF^{\bullet+}$ and $TH^{\bullet+}$, respectively. Interestingly, the standard deviations of the distributions of the spin on a single atom are significantly different (0.013 and 0.037 for TTF and TH, respectively), but the total spin populations of the sulfur atoms are much better defined (standard deviations of 0.007 and 0.014, respectively). Especially for the TH case, this implies that the spin can localize significantly on one atom, however without withdrawing spin density from the carbon atoms.

The instantaneous electronic polarization induced by the oxidation is also shown in Figure 8. The polarization is visualized using the difference density, which we define here as the electron density of the reduced state minus the density

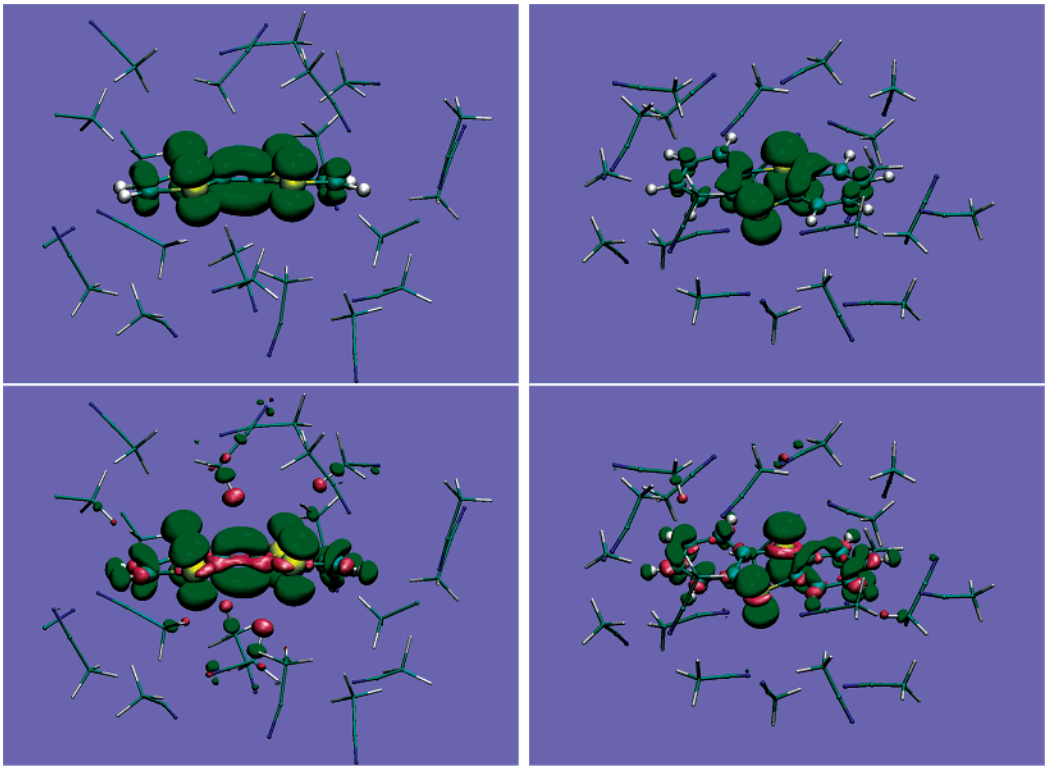

**Figure 8.** Snapshots of TTF (left column) and TH (right column) in solution, with only the closest solvent molecules visualized. The spin density (upper panels) and the difference electron density (lower panels, see text for the definition) are shown at contour levels of +0.002 (green) and −0.002 (pink) au; i.e., green implies an increase of electron density in the reduced state. The difference density illustrates the electronic polarization induced by the cation, in particular of the C−H bonds and first solvation shell. For each solute, the molecular configuration in the upper panel is identical to the configuration in the lower panel. However, the TTF configuration is taken from a trajectory of the neutral molecule while the one for TH represents a radical cation illustrating the different preferential ordering of the solvent molecules. The images are generated with VMD.[73]

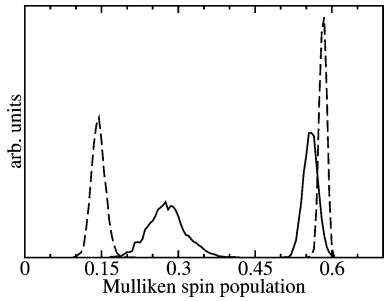


**Figure 9.** Mulliken spin population analysis sampled from all frames of the molecular dynamics simulation of $TTF^{\bullet+}$ (dashed lines) and $TH^{\bullet+}$ (full lines). The two distributions on the left are for the individual sulfur atoms, whereas the distributions on the right are sums of the total population of all sulfur centers in a molecule (4 for TTF and 2 for TH).

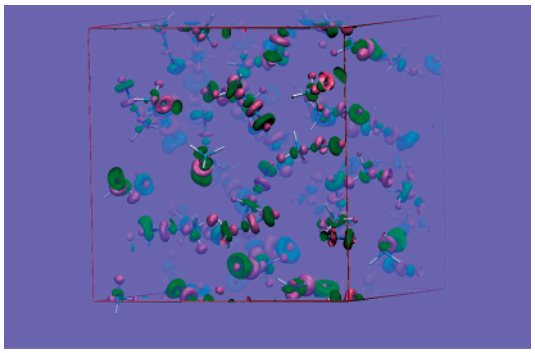

**Figure 10.** Difference between the electron density in the liquid and the gas phase (see text) is shown at contour levels of +0.002 (green) and −0.002 (pink) au. Green implies an increase of electron density in the liquid state. The image is generated with VMD.[73]

of the oxidized state at fixed atomic positions. As expected, the main features reflect the spin density, but the details show the polarization, of the solvent and of the solute itself. A neutral (TTF) and cationic (TH) molecular geometry have been selected, representing two qualitatively different solvent configurations, i.e., with methyl groups or with CN groups preferentially oriented toward the solute. We find that the solvent polarization is in both cases mostly limited to C−H bonds and that the nitrogen lone pair and the C−N triple bond remain unchanged. For comparison, we show in Figure 10 the difference density of the pure solvent, computed as the electron density of the liquid minus the gas-phase density of the individual molecules at their particular geometry. In this case, significant polarization of all groups is observed.

## 6. Redox Potentials

After the structural analysis we now turn to the main objective of this work, namely, the calculation of the redox potentials of TTF and TH using the techniques outlined in section 2.

Vertical energies have been computed for the equilibrated parts of the trajectories, using frames spaced 20 fs apart, i.e., 450 frames and 300 frames from neutral and radical trajectories, respectively. The vertical energies from the neutral to the radical cation states have been computed using three different DFT methods, without SIC and with scaled SIC using $a = 0.1$ and $a = 0.2$. On the basis of these results we can assess the influence of the self-interaction error on the redox potential of the full reaction $TH^{\bullet+} + TTF \rightarrow TH + TTF^{\bullet+}$. The radical cation can be transformed in either the neutral molecule by reduction or

**TABLE 1: Average Vertical Energy Gap $\Delta E_X$, Width $\sigma_X$ of the Gap Fluctuations, and Derived Quantities as Defined in Eqs 6−12 Averaged over a Reduced (X = R) and Oxidized (X = O) Trajectory[a]**

| | $T$ | $\Delta E_R$ | $\sigma_R$ | $\lambda_R$ | $\Delta A_R$ |
|---|---|---|---|---|---|
| $TH \rightarrow TH^{\bullet+}$ | 311.9 (4.2) | 1.722 (05) | 0.182 (00) | 0.613 (07) | 1.109 (12) |
| $TTF \rightarrow TTF^{\bullet+}$ | 302.0 (1.3) | 0.785 (22) | 0.181 (08) | 0.631 (55) | 0.154 (76) |
| $TH^{\bullet+} \rightarrow TH^{2+}$ | 313.3 (0.2) | 2.967 (15) | 0.149 (06) | 0.412 (31) | 2.555 (46) |
| $TTF^{\bullet+} \rightarrow TTF^{2+}$ | 312.2 (0.6) | 2.162 (13) | 0.193 (03) | 0.694 (24) | 1.468 (10) |
| | $T$ | $\Delta E_O$ | $\sigma_O$ | $\lambda_O$ | $\Delta A_O$ |
| $TH^{\bullet+} \rightarrow TH$ | 313.3 (0.2) | 0.360 (13) | 0.150 (06) | 0.417 (34) | 0.777 (21) |
| $TTF^{\bullet+} \rightarrow TTF$ | 312.2 (0.6) | −0.435 (07) | 0.185 (03) | 0.634 (22) | 0.198 (29) |

[a] All radical cation states have been computed using the SIC ($s = 0.2$) method. Temperatures are in kelvin, energies in electronvolts. The estimated error in the last two figures is shown in brackets. For a comparison with experiment, see Table 3.

**TABLE 2: Average Vertical Energy Gap $\Delta E_R$, Width $\sigma_R$ of the Gap Fluctuations, and Derived Quantities as Defined in Eqs 6−12 Averaged over the Trajectory of the Reduced (Neutral) Solute[a]**

| | $T$ | $\Delta E_R$ | $\sigma_R$ | $\lambda_R$ | $\Delta A_R$ |
|---|---|---|---|---|---|
| | | $TH \rightarrow TH^{\bullet+}$ | | | |
| no SIC | 311.9 (4.2) | 2.096 (04) | 0.186 (02) | 0.642 (04) | 1.454 (02) |
| SIC ($a = 0.1$) | 311.9 (4.2) | 1.923 (05) | 0.186 (02) | 0.641 (02) | 1.282 (03) |
| SIC ($a = 0.2$) | 311.9 (4.2) | 1.722 (05) | 0.182 (00) | 0.613 (07) | 1.109 (12) |
| | | $TTF \rightarrow TTF^{\bullet+}$ | | | |
| no SIC | 302.0 (1.3) | 1.121 (21) | 0.180 (08) | 0.623 (58) | 0.498 (80) |
| SIC ($a = 0.1$) | 302.0 (1.3) | 0.960 (21) | 0.181 (08) | 0.626 (57) | 0.334 (78) |
| SIC ($a = 0.2$) | 302.0 (1.3) | 0.785 (22) | 0.181 (08) | 0.631 (55) | 0.154 (76) |

[a] Three different SIC approaches have been employed. Temperatures are in kelvin, energies in electronvolts. The estimated error in the last two figures is shown in brackets. For a comparison with experiment, see Table 3.

**TABLE 3: Computed Free Energy Differences for the Full Reactions Compared to Experimental Results from Ref 74[a]**

| | | $\Delta\Delta A_R$ | | | $\Delta\Delta A_O$ |
|---|---|---|---|---|---|
| | experiment | no SIC | SIC ($a = 0.1$) | SIC ($a = 0.2$) | SIC ($a = 0.2$) |
| $\Delta\Delta A^1$ | −0.93 | −0.956 (0.078) | −0.948 (0.075) | −0.955 (0.064) | −0.579 (0.048) |
| $\Delta\Delta A^2$ | −1.08 | | | −1.087 (0.050) | |

[a] $\Delta\Delta A^1$ gives the result for $TH + TTF^{\bullet+} \rightarrow TH^{\bullet+} + TTF$ (eq 15), and $\Delta\Delta A^2$ for the $TH^{2+} + TTF^{\bullet+} \rightarrow TH^{\bullet+} + TTF^{2+}$ reaction (eq 16). The subscripts R and O denote results obtained as differences of values for $\Delta A_R$ and $\Delta A_O$, respectively (section 3). The estimated error in the last two figures is shown in brackets. The different SIC schemes lead to nearly identical results, illustrating the near perfect cancellation of the self-interaction error for the full reaction.

the dication by oxidation. Both states are spin-paired and described without SIC. The corresponding vertical energy gaps can be computed from the same radical cation trajectory. These vertical energies allow for an independent estimate of the redox potential of $TH^{2+} + TTF^{\bullet+} \rightarrow TH^{\bullet+} + TTF^{2+}$, so that the quality of the harmonic approximation can be investigated. In addition this enables us to estimate the redox potential of the second oxidation step $TH^{2+} + TTF^{\bullet+} \rightarrow TH^{\bullet+} + TTF^{2+}$. The estimators for the corresponding reaction free energies were defined in eqs 15 and 16.

The results for the redox properties of TTF and TH are presented in Tables 1 and 2. In Table 1 all radical cation states are computed using scaled SIC ($a = 0.2$), whereas the effects of the self-interaction correction on the redox properties are summarized in Table 2. As explained in section 3 meaningful comparison of free energies to experiment can only be made for the full reactions because the reference electrode in experiment and in our computer simulations is not the same. Results for the full reactions can be found in Table 3. All computed results have been provided together with an estimate of the statistical error. Since relatively few uncorrelated data points are available we have made a crude estimate of the error as the largest difference between the quantity computed from the full trajectory and the quantity obtained from the first or last half of the data. This analysis shows that results for the full reaction are expected to be statistically accurate within 50−70 meV, which allows for comparison to experiment in a satisfactory manner. As shown in Table 3, excellent agreement with experiment (less than 30 meV error) is obtained for two of the three redox estimates ($\Delta\Delta A_R^1$ and $\Delta\Delta A_R^2$), whereas one result ($\Delta\Delta A_O^1$) is in error by more than 350 meV. The quality of the first two results illustrates the potential of our approach to yield accurate redox potentials using a completely parameter-free approach. However, to ascertain that this method is predictive, it is crucial that the discrepancy between experiment and $\Delta\Delta A_O^1$ is understood.

There are two strong indications that the error in $\Delta\Delta A_O^1$ is not merely due to insufficient statistics. First, it is significantly larger than our estimated statistical error. Second, the same radical cation trajectories and identical configurations are used to estimate both $\Delta\Delta A_R^2$ and $\Delta\Delta A_O^1$, and only one of the two results is in error. This therefore suggests that the error in $\Delta\Delta A_O^1$ must be due to the harmonic approximation. This is indeed confirmed by comparing the $\sigma_R$ and $\sigma_O$ for the half-reactions in Table 1. As explained in section 2 these quantities should be the same if the harmonic approximation is valid. We see that this condition is satisfied for TTF but not for TH. We attribute this to the configurational change (section 5) induced in the TH molecule by oxidation from the neutral to the radical cation state. As discussed previously, this particular conformational change is large, both geometrically and energetically; it can therefore be expected that this cannot simply be treated with the harmonic approximation. This explains why $\Delta\Delta A_O^1$ is in error but in turn raises the question why $\Delta\Delta A_R^1$ is in such good agreement with the experimental result, since the presence of this conformational change could also affect the estimate based

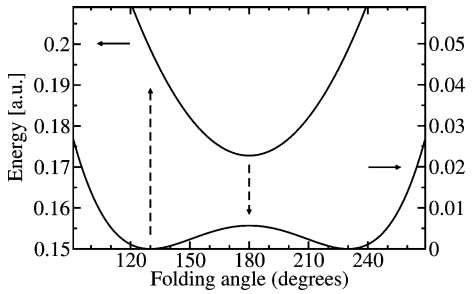


**Figure 11.** Schematic representation of the potential energy surfaces of thianthrene in the reduced (lower curve) and oxidized (upper curve) state as a function of the folding angle (defined in Figure 1). Note the two different *y*-axes, as indicated with the solid arrows. Typical vertical energies computed during MD on the reduced and oxidized surfaces are indicated with dashed arrows pointing up and down, respectively.

on the trajectory in the reduced state. Fortunately, this is not the case, and the asymmetric effect of this conformational change can be explained using the shape of the solute potential energy surface (PES) in the gas phase as a function of the folding angle for both the oxidized and reduced form. A schematic representation of these PESs is given in Figure 11. In the reduced state, the PES has a double-well shape with two equivalent minima for folding angles of approximately 130°, connected by a transition state at the flat geometry (folding angle of 180°). In the oxidized state, a single minimum for a folding angle of 180° is found. A trajectory generated in the oxidized state samples directly from a harmonic potential, but the vertical energies "probe" the transition state region of the reduced PES. Within the harmonic approximation, the transition state region contains therefore no information about the minima of the reduced PES, and an accurate redox estimate based on the harmonic approximation is not possible. A trajectory generated in the reduced state will, for a sufficiently large energy barrier at the transition state, sample one of the equivalent minima, which can then be well approximated using a harmonic approximation. The vertical energies "probe" the oxidized PES, which is harmonic, justifying quadratic extrapolation, and thus we can expect a fairly accurate redox estimate based on the harmonic approximation, consistent with our results in Table 3.

Finally, we discuss the results obtained with the different SIC methods, as shown in Table 2 for the half-reactions and Table 3 for the full reactions. As can be seen in Table 2, the values for $\Delta E_R$ and consequently $\Delta A_R$ change considerably upon introduction of the SIC and also show significant dependence on the value of the parameter $a$. This is expected, as the SIC is a coulomb energy term of a one-electron density. However, there is little effect on the fluctuations of the vertical energy or equivalently on the reorganization free energy (i.e., smaller than 30 meV). However, surprisingly, the differences in $\Delta A_R$ all cancel nearly completely in the estimate of the full reaction, and the final energies are identical to within 10 meV. This is somewhat unexpected since the spin density of both systems has a significantly different spatial extent (see, for example, Figures 8 and 9). This cancellation of self-interaction errors is an advantage that may be specific to calculations of half-reactions where the delocalization is limited to a single solute molecule.

## 7. Conclusions

In this work we have presented ab initio molecular dynamics simulations of liquid acetonitrile, tetrathiafulvalene, and thianthrene in solution. Our analysis shows that, from a computational perspective, acetonitrile is an excellent solvent. Different density functional approximations yield structural and dynamical properties that are similar and in good agreement with previous classical models and experiment. The liquid is mobile at ambient temperature, which results in fast equilibration and good statistics for computed ensemble averages. The interaction of the solvent with two solutes, in the neutral and radical cation state, has been characterized, showing preferential acetonitrile orientation around the solute. A subpicosecond conversion of thianthrene, from a butterfly to a flat shape, is observed upon oxidation. We also compared the solvent polarization induced by oxidizing a solute to the effect of bringing molecules from the gas phase into the liquid phase. This comparison suggests that the latter has a more pronounced effect on molecular polarization, increasing the molecular dipole by 25%.

Redox properties of the solutes have been computed using ab initio molecular dynamics simulations combined with free energy estimates. This detailed modeling describes the interaction of solute and solution explicitly at a high level of theory, incorporating solvent fluctuations and polarization in a consistent and natural way. We find that, for these systems, we can estimate redox potentials based on the harmonic approximation and that a single molecular dynamics simulation, in either the reduced or the oxidized state, can be employed. As the harmonic approximation is an application of Marcus theory, our results can be considered as another confirmation of the validity of linear response. This assumption seems to apply even if the reorganization of the solvent is rather severe on a microscopic level as is exemplified by our obervation of the effective reversal of the orientation of the MeCN molecules in the first solvation shell as a response to the oxidation of the solute. Moreover, when the linear response appeared to break down in the case of thianthrene, which undergoes a significant conformational change upon oxidation, we were still able, using a judicious choice of reference state, to use this approximation. Furthermore, a near perfect cancellation of the self-interaction error is observed for these systems, despite the fact that the spin densities of the solutes are localized in a different way. Excellent agreement with experiment has been obtained for the full redox reactions, demonstrating that these redox properties can now be computed accurately in a parameter-free way.

**Acknowledgment.** One of the authors (J.V.) obtained financial support from a Marie Curie Fellowship. Computer resources were mostly provided by SARA as part of a HPC-Europa grant. Some of the computations were performed on the HPCx facilities at Daresbury Laboratory using an allocation from an Engineering and Physical Sciences Research Council (EPSRC) grant to the United Kingdom Car−Parrinello (UKCP) Consortium.

## References and Notes

(1) Marcus, R. A. *J. Chem. Phys.* **1956**, *24*, 966.
(2) Marcus, R. A. *Rev. Mod. Phys.* **1993**, *65*, 599−610.
(3) Warshel, A. *J. Phys. Chem.* **1982**, *86*, 2218−2224.
(4) Tachiya, M. *J. Phys. Chem.* **1989**, *93*, 7050−7052.
(5) King, G.; Warshel, A. *J. Chem. Phys.* **1990**, *93*, 8682−8692.
(6) Small, D. W.; Matyushov, D. V.; Voth, G. A. *J. Am. Chem. Soc.* **2003**, *125*, 7470−7478.
(7) Blumberger, J.; Sprik, M. *J. Phys. Chem. B* **2004**, *108*, 6529.
(8) Blumberger, J.; Bernasconi, L.; Tavernelli, I.; Vuilleumier, R.; Sprik, M. *J. Am. Chem. Soc.* **2004**, *126*, 3928.
(9) Blumberger, J.; Sprik, M. *J. Phys. Chem. B* **2005**, *109*, 6793.
(10) Tateyama, Y.; Blumberger, J.; Sprik, M.; Tavernelli, I. *J. Chem. Phys.* **2005**, *122*, 234505.
(11) Vassilev, P.; Louwerse, M. J.; Baerends, E. J. *Chem. Phys. Lett.* **2004**, *398*, 212−216.

(12) VandeVondele, J.; Sprik, M. *Phys. Chem. Chem. Phys.* **2005**, *7*, 1363−1367.
(13) Perdew, J. P.; Zunger, A. *Phys. Rev. B* **1981**, *23*, 5048−5079.
(14) Zhang, Y.; Yang, W. *J. Chem. Phys.* **1998**, *109*, 2604−2608.
(15) Sodupe, M.; Bertran, J.; Rodríguez-Santiago, L.; Baerends, E. J. *J. Phys. Chem. A* **1999**, *103*, 166−170.
(16) Grüning, M.; Gritsenko, O. V.; van Gisbergen, S. J. A.; Baerends, E. J. *J. Phys. Chem. A* **2001**, *105*, 9211−9218.
(17) Segura, J. L.; Martín, N. *Angew. Chem., Int. Ed.* **2001**, *40*, 1372−1409.
(18) Demiralp, E.; Goddard, W. A., III *J. Phys. Chem. A* **1997**, *101*, 8128−8231.
(19) Katan, C. *J. Phys. Chem. A* **1999**, *103*, 1407−1413.
(20) Pou-Amérigo, R.; Viruela, P. M.; Viruela, R.; Rubio, M.; Ortí, E. *Chem. Phys. Lett.* **2002**, *352*, 491−498.
(21) Nielsen, S. B.; Nielsen, M. B.; Jensen, H. J. A. *Phys. Chem. Chem. Phys.* **2003**, *5*, 1376−1380.
(22) Katan, C.; Koenig, C.; Blöchl, P. *Comput. Mater. Sci.* **1998**, *10*, 325−329.
(23) Friedrich, R.; Janietz, S.; Wedel, A. *Macromol. Chem. Phys.* **1999**, *200*, 731−738.
(24) Mao, Y.; Thomas, J. K. *J. Org. Chem.* **1993**, *58*, 6641−6649.
(25) Mastryukov, V. S.; Chen, K.-H.; Simonsen, S. H.; Allinger, N. L.; Boggs, J. E. *J. Mol. Struct.* **1997**, *413*, 1−12.
(26) Ito, A.; Ino, H.; Ichiki, H.; Tanaka, K. *J. Phys. Chem. A* **2002**, *106*, 8716−8720.
(27) Kim, S.; Kwon, Y.; Lee, J.-P.; Choi, S.-Y.; Choo, J. *J. Mol. Struct.* **2003**, *655*, 451−458.
(28) Grätzel, M. *Nature* **2001**, *414*, 338−344.
(29) Klein, C.; Nazeeruddin, M. K.; Liska, P.; Di Censo, D.; Hirata, N.; Palomares, E.; Durrant, J. R.; Grätzel, M. *Inorg. Chem.* **2005**, *44*, 178−180.
(30) Böhm, H. J.; McDonald, I. R.; Madden, P. A. *Mol. Phys.* **1983**, *49*, 347−360.
(31) Edwards, D. M. F.; Madden, P. A.; McDonald, I. R. *Mol. Phys.* **1984**, *51*, 1141−1161.
(32) Jorgensen, W. L.; Briggs, J. M. *Mol. Phys* **1988**, *63*, 547.
(33) Cabaleiro-Lago, E. M.; Ríos, M. A. *Mol. Phys.* **1999**, *96*, 309−321.
(34) Grabuleda, X.; Jaime, C.; Kollman, P. A. *J. Comput. Chem.* **2000**, *21*, 901−908.
(35) Fisher, R.; Richardi, J.; Fries, P. H.; Krienke, H. *J. Chem. Phys.* **2002**, *117*, 8467−8478.
(36) Nguyen, T.-N. V.; Peslherbe, G. H. *J. Phys. Chem. A* **2003**, *107*, 1540−1550.
(37) Spångberg, D.; Hermansson, K. *Chem. Phys.* **2004**, *300*, 165−176.
(38) Cabaleiro-Lago, E. M.; Hermida-Ramón, J. M.; Peña-Gallego, A.; Martínez-Núñez, E.; Fernández-Ramos, A. *THEOCHEM* **2000**, *498*, 21−28.
(39) Ford, T. A.; Glasser, L. *Int. J. Quantum Chem.* **2001**, *184*, 226−240.
(40) Mata, R. A.; Cabral, B. J. C. *THEOCHEM* **2004**, *673*, 155−164.
(41) Cichos, F.; Brown, R.; Bopp, P. A. *J. Chem. Phys.* **2001**, *114*, 6824−6833.
(42) Cichos, F.; Brown, R.; Bopp, P. A. *J. Chem. Phys.* **2001**, *114*, 6834−6842.
(43) Pandey, A.; Datta, S. N. *J. Phys. Chem. B* **2005**, *109*, 9066−9072.
(44) Zwanzig, R. W. *J. Chem. Phys.* **1954**, *22*, 1420−1426.
(45) Weisstein, E. W. Cumulant. From MathWorld—A Wolfram Web Resource. http://mathworld.wolfram.com/Cumulant.html (accessed July 2005).
(46) CP2K developers group. http://cp2k.berlios.de/ (accessed July 2005).
(47) VandeVondele, J.; Krack, M.; Mohamed, F.; Parrinello, M.; Chassaing, T.; Hutter, J. *Comput. Phys. Commun.* **2005**, *167*, 103−128.
(48) Lippert, G.; Hutter, J.; Parrinello, M. *Mol. Phys.* **1997**, *92*, 477−487.
(49) Becke, A. D. *Phys. Rev. A* **1988**, *38*, 3098−3100.
(50) Lee, C. T.; Yang, W. T.; Parr, R. G. *Phys. Rev. B* **1988**, *37*, 785−789.
(51) Perdew, J. P.; Burke, K.; Ernzerhof, M. *Phys. Rev. Lett.* **1996**, *77*, 3865−3868.
(52) Goedecker, S.; Teter, M.; Hutter, J. *Phys. Rev. B* **1996**, *54*, 1703−1710.
(53) Hartwigsen, C.; Goedecker, S.; Hutter, J. *Phys. Rev. B* **1998**, *58*, 3641−3662.
(54) VandeVondele, J.; Mohamed, F.; Krack, M.; Hutter, J.; Sprik, M.; Parrinello, M. *J. Chem. Phys.* **2005**, *122*, 014515.
(55) d'Avezac, M.; Calandra, M.; Mauri, F. *Phys. Rev. B* **2005**, *71*, 205210.
(56) Becke, A. D. *J. Chem. Phys.* **1993**, *98*, 5648−5652.
(57) Stephens, P. J.; Devlin, F. J.; Chabalowski, C. F.; Frisch, M. J. *J. Phys. Chem.* **1994**, *98*, 11623−11627.
(58) VandeVondele, J.; Hutter, J. *J. Chem. Phys.* **2003**, *118*, 4365−4369.
(59) Kleinman, L. *Phys. Rev. B* **1981**, *24*, 7412−7414.
(60) Hunt, P.; Sprik, M. *ChemPhysChem* **2005**, *6*, 1805−1808.
(61) Hurle, R. L.; Woolf, L. A. *J. Chem. Soc., Faraday Trans. 1* **1982**, *78*, 2233−2238.
(62) Yeh, I.-C.; Hummer, G. *J. Phys. Chem. B* **2004**, *108*, 15873−15879.
(63) Bopp, T. T. *J. Chem. Phys.* **1967**, *47*, 3621−3626.
(64) Wakai, C.; Saito, H.; Matubayasi, N.; Nakahara, M. *J. Chem. Phys.* **2000**, *112*, 1462−1473.
(65) Marzari, N.; Vanderbilt, D. *Phys. Rev. B* **1997**, *56*, 12847−12865.
(66) Silvestrelli, P. L.; Parrinello, M. *Phys. Rev. Lett.* **1999**, *82*, 3308−3311.
(67) Johnson, R. D., III, Ed. NIST Computational Chemistry Comparison and Benchmark Database, NIST Standard Reference Database Number 101 Release 11, May 2005. http://srdata.nist.gov/cccbdb (accessed July 2005).
(68) Ohba, T.; Ikawa, S. *Mol. Phys.* **1991**, *73*, 985−997.
(69) Larson, S. B.; Simonsen, S. H.; Martin, G. E.; Smith, K.; Puig-Torres, S. *Acta Crystallogr., Sect. C* **1984**, *40*, 103−106.
(70) Aroney, M. J.; Févre, R. J. W. L.; Saxby, J. D. *J. Chem. Soc.* **1965**, 571−575.
(71) Fronza, G.; Ragg, E. *J. Chem. Soc., Perkin. Trans. 2* **1982**, 1209−1211.
(72) Ashton, P. R.; Balzani, V.; Bercher, J.; Credi, A.; Fyfe, M. C. T.; Mattersteig, G.; Menzer, S.; Nielsen, M. B.; Raymo, F. M.; Stoddart, J. F.; Williams, D. J. *J. Am. Chem. Soc.* **1999**, *121*, 3951−3957.
(73) Humphrey, W.; Dalke, A.; Schulten, K. *J. Mol. Graphics* **1996**, *14*, 33−38.
(74) Bard, A. J.; Faulkner, L. R. *Electrochemical Methods, Fundamentals and Applications*, 2nd ed.; John Wiley and Sons: 2001.